Simulations of a High-Pressure Jet

By G. Castiglioni, J. Bellan†, G. Lamanna‡, AND S. Baab‡
California Institute of Technology, Pasadena, CA 91125, USA

Injection and mixing of high-pressure multi-components are key processes for several practical systems used in automotive and aerospace industries. Examples include diesel engines, gas turbines and liquid rocket engines; in all of these devices the pressure of either the fuel or the oxidizer is above critical pressure. Describing the accurate evolution of the mixing process impacts autoignition and, as a consequence, the evolution of the combustion process. Mixing processes at supercritical conditions are strongly characterized by the non-linear coupling between momentum transfer, transport and thermodynamics properties. This work seeks to investigate the thermodynamic state of high-pressure injection of a binary-species system. To this end we performed a two-dimensional simulation of supercritical injection of n-hexane into a nitrogen chamber; in the simulation, all the relevant scales of the system were resolved. The boundary conditions were chosen to overlap with the thermodynamic conditions of the experimental facility of the Institute of Aerospace and Thermodynamics at the University of Stuttgart. A thermodynamic stability analysis was performed to verify the thermodynamic state of the mixing layer. Finally the numerical data was used to investigate the adiabatic mixing assumption typically used in injection modeling.

1. Introduction

Injection and mixing of high-pressure multi-component chemical species are key processes for several practical combustion systems used in automotive and aerospace industries. Examples include diesel engines, gas turbines and liquid rocket engines; in all of these devices the pressure in the combustion chamber is above the critical pressure of the fuel and/or the oxidizer [1]. The processes occurring in the chamber are initiated with mixing, then autoignition and finally combustion occurs. Mixing under these conditions is characterized by the non-linear strong coupling among dynamics, transport and thermodynamics [2]. The main goal of the proposed research is to analyze the thermodynamic stability of a database obtained from Direct Numerical Simulations (DNS) of two species mixing under these conditions and make qualitative and quantitative comparisons with the experimental data provided by the experimental facility of the Institute of Aerospace and Thermodynamics at the University of Stuttgart (ITLR), Germany.

As a preliminary step to fully three-dimensional Direct Numerical Simulations (DNS) we perform a two-dimensional simulation of n-hexane jet injection into a nitrogen-filled chamber at supercritical pressure. The proposed boundary conditions are chosen to overlap with the thermodynamic regimes covered by the experimental facility of ITLR. It is expected that the mixing layer is close to the thermodynamic stability limit with respect

---

† also at Jet Propulsion Laboratory, California Institute of Technology, Pasadena, CA 91109, USA

‡ at the Institute of Aerospace and Thermodynamics, University of Stuttgart, Germany

to phase separation. A stability analysis is performed to verify the thermodynamic state in the mixing layer [3,4].

This report is structured as follows: first a brief review of the ITLR experiment is given. A full description of the code used for the simulations is given in Sec. 3. In high-pressure, multi-species simulations it is important to appreciate the strong influence on the numerical results of the details of the transport models; the transport models are therefore described in Sec. 4. In Sec. 5 the numerical method is briefly summarized. In Sec. 6 a review of the stability criteria is provided. In Sec. 7 the computational results are presented; first the numerical setup is described; a preliminary zero-dimensional stability computation is performed followed by a full field, point-wise stability analysis; additionally the adiabatic mixing assumptions, often used in high-pressure flows to justify simplified transport models is investigated. Finally a summary and conclusions are offered in Sec. 8.

2. Reference experiment

Recent experiments from the Institute of Aerospace and Thermodynamics at the University of Stuttgart [5] are a good example of how a high-pressure fluid can have a different behavior based on the exact thermodynamic conditions. The experiments investigate the high-pressure injection of n-hexane into a nitrogen filled chamber. The chamber is kept at $T_{ch} = 293\,K$ and $p = 5\,MPa$ while the injection temperature is systematically varied and the following values are studied $T_{inj} = 480, 560, 600\,K$. The chamber and injection pressure are supercritical with respect to the pure components critical pressures. The injection temperature range of n-hexane covers a phase space where thermodynamic non-idealities are significant and phase separation is expected for the two lowest T_{inj}. The state of the jet (i.e. single- or two-phase breakup) is investigated with two experimental techniques: parallel-light direct shadowgraphy and planar 90 degree-elastic light scattering (ELS). Details on the experimental setup can be found in Traxinger *et al.* [5] and Baab *et al.* [6].

Shadowgraphy allows for the identification of high-density regions; however, with shadowgraphy it is not possible to distinguish between a liquid and a dense gas. ELS gives more quantitative information, as the intensity of light scattered by particles is measured; the intensity of the signal varies by several orders of magnitude between a single-phase gas and a two-phase flow with embedded droplets; nevertheless, in thermodynamic regimes near phase transition there is still a high degree of uncertainty on whether a particular region of the flow is in two-phase or dense gas phase.

The strong dependence of the thermodynamic regime on the injection temperature is evident in both shadowgraphy and ELS data. At the lowest injection temperature the entirety of the jet appears as a dense region, droplet-like entities are present in the mixing layer and ELS data suggests that the majority of the jet is two-phase state. The situation appears less defined for the $T_{inj} = 560\,K$ case; still the entirety of the jet appears as a dense region in the shadowgraph, the droplet-like features are no longer present, but the range of intensity signal from ELS is similar to the lower injection temperature case at some distance downstream of the nozzle. These observations seem to suggest that there are flow regions in the two-phase state, but there could be regions in the dense gas phase as well. The highest injection temperature case is also non-trivial to interpret; the jet exhibits a dense core region up to around 30 nozzle diameters from the injection point; afterward, the extent of the darkness decreases significantly. ELS data shows that there is little scattering, suggesting that a liquid phase might no longer be present.

3. Governing equations

3.1. *Conservation equations*

The following conservation equations are solved numerically

$$\frac{\partial \rho}{\partial t}+\frac{\partial}{\partial x_j}(\rho u_j)=0, \tag{3.1}$$

$$\frac{\partial(\rho u_i)}{\partial t}+\frac{\partial}{\partial x_j}\left(\rho u_i u_j+p\delta_{ij}-\sigma_{ij}\right)=0, \tag{3.2}$$

$$\frac{\partial(\rho e_t)}{\partial t}+\frac{\partial}{\partial x_j}\left[(\rho e_t+p)u_j-u_i\sigma_{ij}+q_j\right]=0, \tag{3.3}$$

$$\frac{\partial(\rho Y_\alpha)}{\partial t}+\frac{\partial}{\partial x_j}\left(\rho Y_\alpha u_j+J_{\alpha j}\right)=0, \tag{3.4}$$

where t is time, x_i are the Cartesian coordinates (subscripts $i,j\in[1,3]$), ρ is the mixture average density, u_i the mass average velocities, p is the pressure, $e_t=e+u_iu_i/2$ is the total energy with e being the internal energy. Y_α is the mass fraction of species α (subscript $\alpha\in[1,N-1]$ with N number of species, note that Greek subscripts do not follow Einstein notation). σ_{ij} is the Newtonian viscous stress tensor

$$\sigma_{ij}=\mu\left(2S_{ij}-\tfrac{2}{3}S_{kk}\delta_{ij}\right), \quad S_{ij}=\frac{1}{2}\left(\frac{\partial u_i}{\partial x_j}+\frac{\partial u_j}{\partial x_i}\right), \tag{3.5}$$

where μ is the viscosity, $J_{\alpha i}$ is the mass flux, relative to the mass average velocity, of species α in direction i, and q_i is the heat flux. The mass and heat flux vectors are based on full matrices of mass-diffusion coefficients and thermal-diffusion factors of Harstad and Bellan [7]

$$J_{\alpha j}=-\rho\left[Y_\alpha\left(D_{T,\alpha}\right)\frac{1}{T}\frac{\partial T}{\partial x_j}+Y_\alpha\left(D_{p,\alpha}\right)\frac{1}{p}\frac{\partial p}{\partial x_j}+\sum_{\beta=1}^{N-1}\left(D'_{\alpha\beta}\frac{m_\alpha}{m_\beta}\right)\frac{\partial Y_\beta}{\partial x_j}\right], \tag{3.6}$$

$$q_j=-\lambda\frac{\partial T}{\partial x_j}+\sum_{\alpha=1}^{N-1}J_{\alpha j}\left[\left(\frac{h_\alpha}{m_\alpha}-\frac{h_N}{m_N}\right)-R_uT\left(\frac{\bar{\alpha}^b_{T,\alpha}}{m_\alpha}-\frac{\bar{\alpha}^b_{T,N}}{m_N}\right)\right]. \tag{3.7}$$

where

$$D_{T,\alpha}=-\sum_{\beta=1}^{N}\bar{\alpha}^b_{T,\beta}F_{\beta\alpha}, \qquad D_{p,\alpha}=\frac{p}{R_uT}\sum_{\beta=1}^{N}v_\beta F_{\beta\alpha}, \tag{3.8}$$

$$D_{\alpha\gamma}=\sum_{\beta=1}^{N}F_{\alpha\beta}\alpha_{D\beta\gamma}, \tag{3.9}$$

$$\bar{\alpha}^b_{T,\alpha}=\sum_{\beta=1}^{N}X_\beta\alpha^b_{T,\beta\alpha}, \tag{3.10}$$

$$D'_{\alpha\beta} = D_{\alpha\beta} - \left(1 - \frac{m_\beta}{m_N}\right)\left(\sum_{\gamma=1}^{N-1} D_{\alpha\gamma} X_\gamma\right). \tag{3.11}$$

Here, $X_\alpha = Y_\alpha m / m_\alpha$ represents the molar fraction; T is the temperature; m_α is the species molar mass; m is the mixture molar mass, $m = \sum_{\gamma=1}^{N} m_\gamma X_\gamma$; $v_\alpha = (\partial v / \partial X_\alpha)_{T,p,X_\beta(\beta \neq \alpha)}$ is the partial molar volume, where the molar volume is $v = 1/n$ and $n = \rho/m$ is the molar density; $h_\alpha = (\partial h / \partial X_\alpha)_{T,p,X_\beta(\beta \neq \alpha)}$ is the partial molar enthalpy, where the molar enthalpy is $h = G - T(\partial G / \partial T)_{p,X}$ with G being the Gibbs energy; R_u is the universal gas constant; $D_{\alpha\gamma}$ are the pairwise mass diffusion coefficients; $\alpha^b_{T,\alpha\beta}$ are the binary thermal diffusion factors; and λ is the thermal conductivity. The mass-diffusion factors, $\alpha_{D\alpha\beta}$, are calculated from thermodynamics as

$$\alpha_{D\alpha\beta} \equiv \frac{1}{R_u T} X_\alpha \frac{\partial \mu_\alpha}{\partial X_\beta} = (\delta_{\alpha\beta} - \delta_{\alpha N}) + X_\alpha (R_{\alpha\beta} - R_{\alpha N}), \quad 1 \leq \alpha \leq N,\ 1 \leq \beta \leq N-1 \tag{3.12}$$

$$R_{\alpha\beta} \equiv \frac{\partial \ln \gamma_\alpha}{\partial X_\beta}, \qquad 1 \leq \alpha \leq N,\ 1 \leq \beta \leq N \tag{3.13}$$

where μ_α is the chemical potential of species α written in terms of $N-1$ species; $\gamma_\alpha \equiv \varphi_\alpha / \varphi^o_\alpha$ where φ is the fugacity coefficient written in terms of N species and the superscript o denotes the pure ($X_\alpha = 1$) limit. Matrix elements $F_{\beta\gamma}$ are the solution of the mixing rules equations [7]

$$\sum_{\beta=1}^{N} \left[\delta_{\alpha\beta} - (1 - \delta_{\alpha\beta}) X_\beta \frac{\bar{\mathcal{D}}_\alpha}{\mathcal{D}^b_{\alpha\beta}}\right] \frac{F_{\beta\gamma}}{X_\beta} = \bar{\mathcal{D}}_\alpha \frac{(\delta_{\alpha\gamma} - Y_\alpha)}{X_\alpha} \tag{3.14}$$

where

$$\bar{\mathcal{D}}_\alpha = 1 / \sum_{\substack{\beta=1 \\ \beta \neq \alpha}}^{N} \left(\frac{X_\beta}{\mathcal{D}^b_{\alpha\beta}}\right). \tag{3.15}$$

Solutions for $F_{\beta\gamma}$ may be obtained by an approximate inversion [8] as follows:

$$F_{\beta\gamma} \simeq X_\beta F^{(1)}_{\beta\gamma}, \tag{3.16}$$

$$F^{(1)}_{\alpha\beta} = \frac{(1 + Y_\alpha)}{X_\alpha} \mathcal{D}^*_\alpha \delta_{\alpha\beta} + (1 - \delta_{\alpha\beta}) \frac{\mathcal{D}^*_\alpha \mathcal{D}^*_\beta}{\mathcal{D}^b_{\alpha\beta}} - \left(\sigma_\alpha \mathcal{D}^*_\alpha + \sigma_\beta \mathcal{D}^*_\beta\right) + \sum_{\gamma=1}^{N} \left(Y_\gamma \sigma_\gamma \mathcal{D}^*_\gamma\right), \tag{3.17}$$

$$\mathcal{D}^*_\alpha = (1 - Y_\alpha) \bar{\mathcal{D}}_\alpha, \tag{3.18}$$

$$\sigma_\alpha = \frac{m_\alpha}{m} (1 + Y_\alpha) + \sum_{\substack{\beta=1 \\ \beta \neq \alpha}}^{N} Y_\beta \frac{\mathcal{D}^*_\beta}{\mathcal{D}^b_{\alpha\beta}} \tag{3.19}$$

where $\mathcal{D}^b_{\alpha\beta}$ is the full approximation binary-diffusion matrix. This method leads to a singularity when the mixture is composed of only one species (as, for instance, in pure fuel zones). In that case equation (3.15) is no longer used and the diffusion coefficients are evaluated by means of the binary-diffusion matrix, by setting $\mathcal{D}^*_\alpha = \mathcal{D}^b_{\alpha N}$ where N represents the index associated with the solvent. This method was tested against an exact Gauss inversion (not shown) and it gave the same results, with an additional gain in computational time. Defining $\mathcal{D}_{\alpha\beta}$ as the first approximation of the binary diffusion matrix and realizing that the deviation of the ratio $\mathcal{D}^b_{\alpha\beta} / \mathcal{D}_{\alpha\beta}$ from unity is comparable to uncertainties in binary diffusion coefficients values [7], we assume $\mathcal{D}^b_{\alpha\beta} = \mathcal{D}_{\alpha\beta}$. The computation of $\mathcal{D}_{\alpha\beta}$ and $\alpha^b_{T,\alpha\beta}$ is described in Sec. 4.3 along with the other transport properties. The system of conservation equations consisting of the mass, momentum, total energy, and species mass differential equations is coupled to the Peng-Robinson equation of state (EOS) used in conjunction with a volume shift for improved accuracy [9].

3.2. *Equation of state*

Equations (3.1)-(3.4) are coupled with the Peng-Robinson (PR) EOS

$$p = \frac{R_u T}{(v_{pr} - b_{mix})} - \frac{a_{mix}}{\left(v_{pr}^2 + 2b_{mix}v_{pr} - b_{mix}^2\right)} \tag{3.20}$$

from which T and p are obtained as an iterative solution which satisfies both values of density and of internal energy, as obtained from the conservation equations. Here v_{pr} is the molar PR volume, and $v = v_{pr} + v_s$ where v_s is the volume shift introduced so as to improve the accuracy of the PR EOS at high p; a_{mix} and b_{mix} are functions of T and X_i and are defined as follows

$$a_{mix} = \sum_\alpha \sum_\gamma X_\alpha X_\gamma a_{\alpha\gamma}(T), \;\; b_{mix} = \sum_\alpha X_\alpha b_\alpha, \tag{3.21}$$

where indices do not follow the Einstein notation, and

$$a_{\alpha\gamma} = (1 - k'_{\alpha\gamma})\sqrt{\alpha_{\alpha\alpha}\alpha_{\gamma\gamma}}, \tag{3.22}$$

$$\alpha_{\alpha\alpha}(T) \equiv 0.457236(R_u T_{c,\alpha})^2 \times \frac{\left[1 + c_\alpha(1 - \sqrt{T_{red,\alpha}})\right]^2}{p_{c,\alpha}}, \tag{3.23}$$

$$c_\alpha = 0.37464 + 1.54226\Omega_\alpha - 0.26992\Omega_\alpha^2, \tag{3.24}$$

where $T_{red,\alpha} \equiv T/T_{c,\alpha}$, $T_{c,\alpha}$ is the critical temperature and Ω_α is the acentric factor. Also,

$$b_\alpha = 0.077796\frac{R_u T_{c,\alpha}}{p_{c,\alpha}}, \tag{3.25}$$

$$T_{c,\alpha\gamma} = (1 - k_{\alpha\gamma})\sqrt{T_{c,\alpha}T_{c,\gamma}} \text{ with } k_{\alpha\alpha} = 0, \tag{3.26}$$

$$v_{c,\alpha\gamma} = \frac{1}{8}\left(v_{c,\alpha}^{1/3} + v_{c,\gamma}^{1/3}\right)^3, \quad Z_{c,\alpha\gamma} = \frac{1}{2}\left(Z_{c,\alpha} + Z_{c,\gamma}\right), \quad p_{c,\alpha\gamma} = \frac{R_u T_{c,\alpha\gamma} Z_{c,\alpha\gamma}}{v_{c,\alpha\gamma n}} \tag{3.27}$$

with $T_{red,\alpha\gamma} \equiv T/T_{c,\alpha\gamma}, Z_{c,\alpha}$ being the critical compression factor with the compression factor defined as $Z = p/(\rho T R_u/m)$, $v_{c,\alpha}$ being the critical volume, and $p_{c,\alpha}$ being the critical pressure. $k_{\alpha\gamma}$ is an empirical mixing parameter. The relationship between parameters $k_{\alpha\gamma}$ and $k'_{\alpha\gamma}$ is

$$(1 - k_{\alpha\gamma}) = (1 - k'_{\alpha\gamma})\frac{(v_{c,\alpha}v_{c,\gamma})^{1/2}}{v_{c,\alpha\gamma}}\frac{Z_{c,\alpha\gamma}}{\sqrt{Z_{c,\alpha}Z_{c,\gamma}}}. \tag{3.28}$$

Values of $k'_{\alpha\gamma}$ are obtained from [10] otherwise $k'_{\alpha\gamma} = 0$ is used. Details about the volume shift implementation can be found in [1] and references therein.

4. Transport models

4.1. *Mixture viscosity*

To compute the individual species viscosity, μ_α, the Lucas method [11] has been selected due to its high-p-accuracy capabilities. To compute the mixture physical viscosity, μ_{ph}, the Wilke method [11] is utilized providing

$$\mu_{ph} = \sum_{\alpha=1}^{N} X_\alpha \omega_\alpha^M \mu_\alpha \tag{4.1}$$

$$(\omega_\alpha^M)^{-1} = \sum_{\beta=1}^{N} \phi_{\alpha\beta} X_\beta \tag{4.2}$$

$$\phi_{\alpha\beta} = \frac{\left[1 + (\mu_\alpha/\mu_\beta)^{1/2}(m_\beta/m_\alpha)^{1/4}\right]^2}{\left[8(1 + m_\alpha/m_\beta)\right]^{1/2}} \tag{4.3}$$

where ω_α^M are weighting factors [11].

4.2. *Mixture thermal conductivity*

To compute the physical mixture thermal conductivity, λ_{ph}, first the species conductivities λ_α are calculated using the Stiel-Thodos method [11], and then the Wassiljewa-Mason-Saxena method ([11]) is utilized to compute λ_{ph} from λ_α as

$$\lambda_{ph} = \sum_{\gamma=1}^{N} X_\alpha \omega_\alpha^Q \lambda_\alpha \tag{4.4}$$

where

$$\omega_\alpha^Q = \omega_\alpha^M. \tag{4.5}$$

4.3. *Binary mass diffusivities*

Matrix elements $\mathcal{D}_{\alpha\gamma}^b$ are the building blocks of $F_{\alpha\gamma}$ and ultimately of $D'_{\alpha\gamma}$. To compute $\mathcal{D}_{\alpha\gamma}^b = \mathcal{D}_{\alpha\gamma}$, we adopt the method of [12] which gives (in cgs units)

$$n\mathcal{D}_{\alpha\gamma} = 2.81 \times 10^{-5} \frac{f_{D,\alpha\gamma}(T)}{r_D v_{c,\alpha\gamma}^{2/3}} \left[\left(\frac{1}{m_\alpha} + \frac{1}{m_\gamma}\right) T\right]^{1/2} \tag{4.6}$$

where $f_{D,\alpha\gamma}(T)$ is generically defined for each matrix element as $f_D(T) \equiv (T_{red})^s$ with $\ln s = \sum_{\zeta=0}^{5} a_\zeta^s (\ln T_{red})^\zeta$ where the a^s vector has elements {-0.84211, -0.32643, -0.10053, 0.07747, 0.0127, -0.00995}, and r_D is a constant $O(1)$ which provides an empirical adjustment for the specifics of the collisional interactions of a selected pair of species. $T_{red,\alpha\gamma} \equiv T/T_{c,\alpha\gamma}$. Values of r_D are listed elsewhere [12] for species pairs relevant to combustion.

4.4. *Binary thermal diffusion factors*

According to Harstad and Bellan [7]

$$\alpha_{T,\alpha\gamma}^b = \zeta_{\alpha\gamma} \frac{(m_\alpha \omega_\gamma^T - m_\gamma \omega_\alpha^T)}{(m_\alpha + m_\gamma)\mathcal{D}_{\alpha\gamma}} \tag{4.7}$$

$$\omega_\alpha^T = \frac{\omega_\alpha^Q \lambda_\alpha}{R_u n}, \quad \zeta_{\alpha\gamma} = \frac{6}{5} C_{\alpha\gamma}^* - 1 \tag{4.8}$$

where ω_{α}^{Q} is computed from equations (4.2) and (4.5), and $C^{*}_{\alpha\gamma}$ is given by [13] and is function of a normalized temperature including the characteristic molecular interaction potential [7].

5. Numerical method

Equations (3.1)-(3.4) are discretized using a compact 6th order finite difference scheme [14] with a classical fourth-order explicit Runge-Kutta time integration. The high-order scheme is stabilized with the 6th order compact filter of Gaitonde and Visbal [15] with $\alpha = 0.35$.

6. Stability analysis

The spinodal locus is characterized by the conditions in which a macroscopic system becomes unstable. For pure substances the instability is simultaneously mechanical and thermal [4]. For example, in pure substances near the critical point the density can have unbounded fluctuations. Unlike for pure substances, multicomponent mixtures have composition fluctuations [4], and thus the instability in this case is of thermodynamic nature rather than mechanical. This type of instability is called diffusional or material instability. The stability condition for a multicomponent mixture is [3, 4]

$$-\left(\frac{\partial \mu_i}{\partial N_i}\right)_{T,P,N_j(i\neq j)} > 0 \tag{6.1}$$

where μ_i is the chemical potential of species i and N_i is the number of molecules of component i. Whenever equation (6.1) is violated a multicomponent system undergoes phase separation. Computing the stability condition allows for the detection of unstable thermodynamic regions which lead to phase separation. Phase separation can lead to strong density gradients which can enhance vorticity production [16]. Computing the stability condition from Eq. (6.1) for a pressure-explicit EOS is costly as it involves the calculation of the first and second derivative with respect to the number of moles and the derivative with respect to volume, V . Another method, computationally less expensive, has been proposed in the past by Heidemann and Khalil [17] and it is what it is adopted here. A necessary condition for a point to lie on the limit of stability is that the Hessian, $\mathbf{Q}$, of the Helmholtz free energy

$$Q_{\alpha\beta} = \frac{\partial^2 A}{\partial n_\beta \partial n_\alpha}, \tag{6.2}$$

should have a null determinant. The stability condition is therefore given by the condition

$$\det \mathbf{Q} > 0, \tag{6.3}$$

where

$$Q_{\alpha\beta} = \left(\frac{\partial^2 A}{\partial n_\alpha \partial n_\beta}\right)_{T,V} = R_u T \left(\frac{\partial\ log f_\alpha}{\partial n_\beta}\right)_{T,V}, \tag{6.4}$$

where f_α is the fugacity.

7. Results

7.1. *Configuration and boundary conditions*

The computational setup mimics the thermodynamic conditions of one of the experiments described in Traxinger *et al.* [5] and that were performed at ITLR. Supercritical n-hexane at $T_{inj} = 600\,K$ is injected in a nitrogen filled chamber at $T_{ch} = 293\,K$ and $p = 5\,MPa$. In order to allow for DNS, the injection Reynolds number based on the centerline velocity and jet diameter is kept at $Re = 2000$. Preliminary two-dimensional simulations have been carried out. The domain size is $50D \times 28D$ in the x_1 and x_2 directions respectively, x_1 being the streamwise direction; the jet diameter is $D = 0.00236\,m$. The boundary conditions are one-dimensional real-gas EOS Navier Stokes Characteristic Boundary Conditions [18,19]. Additionally, to suppress spurious numerical reflections from the outflow boundaries, a sponge layer was added to the outflow boundaries [20]. The penalty term is cubic and the sponge thickness is of $8D$ and $5D$ in the x_1 and x_2 directions, respectively. The inlet velocity profile is specified by an hyperbolic tangent function

$$u_1 = \frac{U_0}{2}\left[1 - tanh\left(\frac{r - r_{jet}}{2\delta}\right)\right] \;\; ; \;\; u_2 = 0 \tag{7.1}$$

where U_0 is the centerline velocity, $r = x_2$, $r_{jet} = D/2$ is the jet radius, and $\delta = 0.05D$ is the initial shear layer thickness. Similar hyperbolic tangent functions are used to impose the mass fraction and temperature inlet profiles. The grid is Cartesian and it is generated with hyperbolic stretching to cluster points towards the centerline. The grid resolution is 1024×512 points in the x_1 and x_2 directions respectively. The hyperbolic tangent profile is discretized with approximately 46 points between the regions of steep variation.

7.2. *Preliminary stability investigation*

Towards the goal of determining the thermodynamic regime during the high-pressure injection of n-hexane into a nitrogen filled chamber, some preliminary zero-dimensional evaluations are performed based on injection and chamber conditions. In a very approximate manner, it could be expected that in the mixing layer the molar composition sweeps from pure nitrogen to pure n-hexane (injectant). Also, temperatures can be expected to be in the range $300 - 600\,K$. In Figure 1 the spinodal locus for a mixture of nitrogen/n-hexane is plotted together with four isotherms ($300\,K$, $400\,K$, $500K$, and $600\,K$). The sub-figures (a), (b), (c) corresponds to different molar fractions, respectively $X_{N2} = 0.1, 0.5, 0.9$. The isotherms are colored by the thermodynamic stability criteria (equation 6.1), i.e. red is unstable while blue is stable. Sub-figures (a), (b), and (c), have molar composition that are representative of the inner edge, of the core, and of the outer edge of the mixing layer respectively. For pressures around $5\,MPa$, temperatures in the range $350 - 450\,K$, and mixture fractions in the range $X_{N2} = 0.4 - 0.6$, the mixture could be below the spinodal limit.

7.3. *Two-dimensional results*

As a step towards three-dimensional DNS, two-dimensional computations have been performed. In Fig. 2 instantaneous snapshots of the density field (above) and the stability criteria (below) taken at the same time are shown. The two-dimensional density field can be used for a qualitative comparison with the shadowgraphy pictures of the experimental results. Similarly to the experimental results, the jet exhibits a dense gas core (dark region) of approximately $15D$ after which the density decreases significantly due to mixing effects. However, density alone provides no information on the thermody-

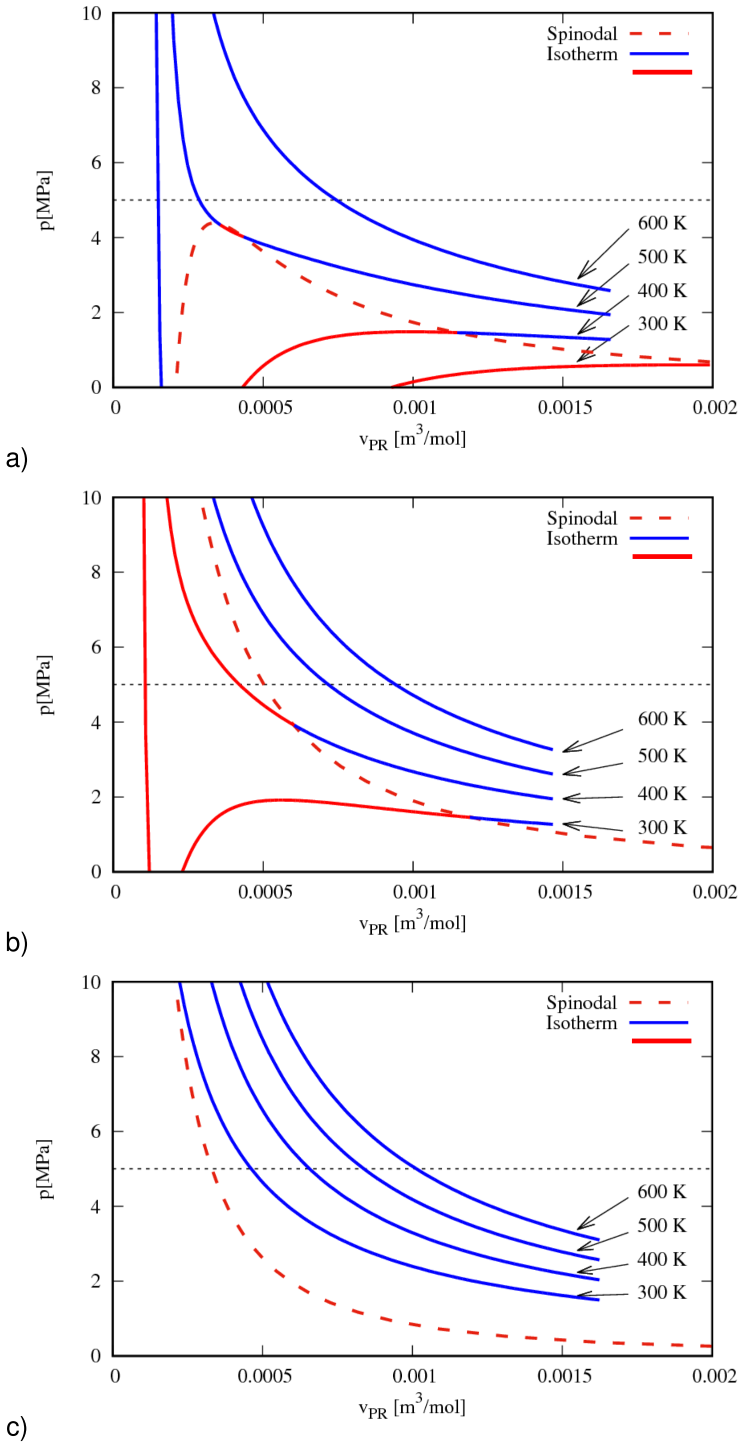

FIGURE 1. A priori stability analysis of a mixture of nitrogen and n-hexane. Plotted are the spinodal (dashed line) and four isotherms (solid line) for different mixture compositions. The isotherms are colored by thermodynamic stability, i.e. red is unstable while blue is stable.

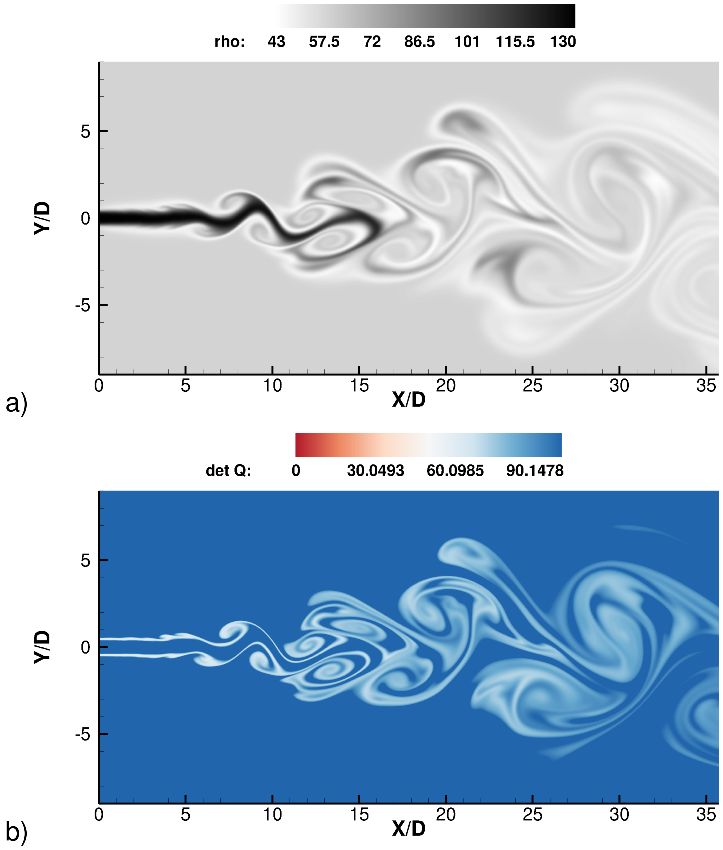

FIGURE 2. Instantaneous snapshot of two-dimensional density field a), and stability field b) at the same time, t_0.

namic state. The point-wise stability criterion value, shown in Fig. 2 b), is everywhere positive indicating that the fluid is in single phase, dense gas state. The value of the stability criterion decreases significantly in the shear and mixing layers indicating that these regions are significantly closer to the stability limit than the chamber and jet core regions.

7.4. *Mixing*

Recent numerical computations of Traxinger *et al.* [5] seem to support the validity of the adiabatic mixing assumption for the simulation of high-pressure injection. Under the assumptions of homogeneous system, steady state, adiabatic mixing, and when using mass and enthalpy conservation equations, one can derive an expression for the enthalpy of a binary mixture [5, 21]

$$h_{mix}(T_{mix}) = X_1 h_1(T_1) + (1 - X_1) h_2(T_2) + h_{excess}(T_{mix}) \tag{7.2}$$

where h_{excess} is the difference between the mixture enthalpy and the ideal gas mixture enthalpy $X_1 h_1(T_1) + (1 - X_1) h_2(T_2)$; h_{excess} is computed from the NIST database [22]. Equation (7.2) gives a functional relation between the mixture fraction of a component (X_1) and the mixture temperature (T_{mix}). Even though Eq. (7.2) includes real gas effects, it neglects the effect of irreversibilities due to the mixing of two fluids with large differences in temperature and chemical composition. A snapshot of the two-dimensional field has been used to investigate the adiabatic mixing assumption. In Fig. 3 the locus expressed by Eq. (7.2) (black line) is plotted in the (T,$y_{n-hexane}$) plane together with the Vapor-Liquid Equilibrium (VLE) locus (blue line) and the two-dimensional simulation phase space (red dots). The adiabatic mixing locus and the two-dimensional simulations states lie above the VLE locus, both indicating single phase regime. In contrast to the simulations of Traxinger *et al.* the adiabatic mixing locus does not accurately represent the simulation states. The simulation states show a certain degree of spreading indicating the presence of non-idealities typical of high-pressure flows.

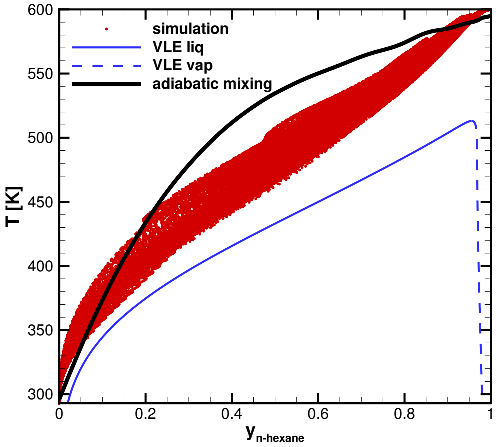

FIGURE 3. Adiabatic mixing (black line), VLE (blue line) loci plotted together with the thermodynamic states (T,$y_{n-hexane}$) of two-dimensional simulation (red dots).

8. Conclusions

The goal of this project is to investigate numerically the thermodynamic regime of high-pressure injection of n-hexane into a nitrogen filled chamber. The thermodynamic conditions are chosen to overlap the thermodynamic conditions of the recent experiments conducted at ITLR [5]. As an exploratory study before conducting fully three-dimensional DNS, two-dimensional computations have been performed and a rough qualitative comparison based on density shows similar features to the experimental results, although the jet core length appears to be shorter.

Preliminary zero-dimensional computations do not conclusively indicate if, for a specified injection temperature and the chamber conditions of interest, the fluid is in a single phase or two phase regime. However, this simple preliminary estimate suggests that the thermodynamic regime of interest is close to the stability limit and that two phase regions may be expected. In particular, for a chamber pressure of $p = 5MPa$ and a molar fraction of nitrogen of $X_{N2} = 0.5$, if the local mixture temperature decreases below $450\,K$ then there could be regions of thermodynamic instability. Clearly, it is necessary to compute the stability criteria pointwise in flow fields generated by two-, three-dimensional computations in order to know the thermodynamic regime. Full two-dimensional field stability analysis shows that, according to our computations, the flow field is everywhere in single phase regime (dense gas).

Finally, a commonly used assumption of adiabatic mixing was investigated. Recent experiments by Traxinger *et al.* seem to suggest that this strong assumption holds remarkably well even for high-pressure flows. From our simulations, it seems that adiabatic mixing is not a good assumption. Our computations employ a full transport model which includes baro- and thermo-diffusion effects; on the contrary, Traxinger *et al.* employ a Fickian diffusion model without accounting for baro- and thermo-diffusion effects. Our preliminary results seem to suggest that it is necessary to use a full transport model to capture properly the non-adiabatic mixing effects and that these effects are not negligible. The conclusions presented here cannot be considered definitive as with three-dimensional effect, i.e. turbulence, and higher Reynolds numbers the turbulent mixing (in particular the stirring effect) can hasten and homogenize the macroscopic mixing process. Three-dimensional simulations are currently ongoing and high Reynolds number Large Eddy Simulations are planned in the future.

Acknowledgments

The authors gratefully acknowledge the hospitality of faculty and staff of Lehrstuhl für Aerodynamik und Strömungsmechanik, Technische Universität München. Financial support has been provided by the German Research Foundation (Deutsche Forschungsgemeinschaft – DFG) in the framework of the Sonderforschungsbereich Transregio 40. Support for the first two authors has also been provided by the U.S. Army Research Office under the direction of Dr. Ralph Anthenien. The computational resources were provided by the NASA Advanced Supercomputing at Ames Research Center under the T3 program directed by Dr. Michael Rogers.

References

[1] MASI, E., BELLAN, J., HARSTAD, K.G. AND OKONG'O, N.A. (2013). Multi-species turbulent mixing under supercritical-pressure conditions: modelling, direct numerical simulation and analysis revealing species spinodal decomposition. *J. Fluid Mech.*, **721**, 578–626.

[2] MÜLLER, H., NIEDERMEIER, C.A., MATHEIS, J., PFITZNER, M. AND HICKEL, S. (2016). Large-eddy simulation of nitrogen injection at trans-and supercritical conditions. *Phys. Fluids*, **28**(1), 015102.

[3] TESTER, J.W. AND MODELL, M. (1997). *Thermodynamics and its Applications*. Prentice Hall PTR.

[4] DEBENEDETTI, P.G. (1996). *Metastable liquids: concepts and principles*. Princeton University Press.

[5] TRAXINGER, C., MÜLLER, H., PFITZNER, M., BAAB, S., LAMANNA, G., WEIGAND, B., MATHEIS, J., STEMMER, C., ADAMS, N.A. AND HICKEL, S. (2017). Experimental and numerical investigation of phase separation due to multi-component mixing at high-pressure conditions. *arXiv preprint arXiv:1706.03923*.

[6] BAAB, S., FÖRSTER, F., LAMANNA, G. AND WEIGAND, B. (2016). Speed of sound measurements and mixing characterization of underexpanded fuel jets with supercritical reservoir condition using laser-induced thermal acoustics. *Experiments in Fluids*, **57**(11), 172.

[7] HARSTAD, K.G. AND BELLAN, J. (2004). Mixing rules for multicomponent mixture mass diffusion coefficients and thermal diffusion factors. *J. Chem. Phys.*, **120**(12), 5664–5673.

[8] ERN, A. AND GIOVANGIGLI, V. (1998). Thermal diffusion effects in hydrogen-air and methane-air flames. *Combustion Theory and Modelling*, **2**(4), 349–372.

[9] HARSTAD, K.G., MILLER, R.S. AND BELLAN, J. (1997). Efficient high-pressure state equations. *AIChE J.*, **43**(6), 1605–1610.

[10] KNAPP, H., DÖRING, R., OELLRICH, L., PLÖCKER, U. AND PRAUSNITZ, J.M. (1982). *Vapor-liquid equilibria for mixtures of low boiling substances*, vol. VI. Dechema.

[11] POLING, B.E., PRAUSNITZ, J.M. AND O'CONNELL, J.P. (2001). *The properties of gases and liquids*. McGraw-Hill,.

[12] HARSTAD, K. AND BELLAN, J. (2004). High-pressure binary mass diffusion coefficients for combustion applications. *Industrial & engineering chemistry research*, **43**(2), 645–654.

[13] HIRSCHFELDER, J., BIRD, R.B. AND CURTISS, C.F. (1964). Molecular theory of gases and liquids.

[14] LELE, S.K. (1992). Compact finite difference schemes with spectral-like resolution. *J. comp. phys.*, **103**(1), 16–42.

[15] GAITONDE, D.V. AND VISBAL, M.R. (1998). *High-order schemes for Navier-Stokes equations: algorithm and implementation into FDL3DI*. Tech. rep., Air Force Research Lab Wright-Patterson AFB OH Air Vehicles Directorate.

[16] HANNOUN, I.A., FERNANDO, H.J.S. AND LIST, E.J. (1988). Turbulence structure near a sharp density interface. *J. Fluid Mech.*, **189**, 189–209.

[17] HEIDEMANN, R.A. AND KHALIL, A.M. (1980). The calculation of critical points. *AIChE J.*, **26**(5), 769–779.

[18] OKONG'O, N. AND BELLAN, J. (2002). Consistent boundary conditions for multicomponent real gas mixtures based on characteristic waves. *J. of Comp. Phys.*, **176**(2), 330–344.

[19] YOO, C.S., WANG, Y., TROUVÉ, A. AND IM, H.G. (2005). Characteristic boundary conditions for direct simulations of turbulent counterflow flames. *Combustion Theory and Modelling*, **9**(4), 617–646.

[20] MANI, A. (2012). Analysis and optimization of numerical sponge layers as a nonreflective boundary treatment. *J. Comput. Phys.*, **231**(2), 704–716.

[21] QIU, L. AND REITZ, R.D. (2015). An investigation of thermodynamic states during high-pressure fuel injection using equilibrium thermodynamics. *International Journal of Multiphase Flow*, **72**, 24–38.

[22] LEMMON, E.W., HUBER, M.L. AND MCLINDEN, M.O. (2002). Nist reference fluid thermodynamic and transport properties–refprop.